Factors Affecting Competitive Ion−Molecule Reactions: $ClO^- + C_2H_5Cl$ and C_2D_5Cl via E2 and S_N2 Channels

Wei-Ping Hu and Donald G. Truhlar*

Contribution from the Department of Chemistry and Supercomputer Institute, University of Minnesota, Minneapolis, Minnesota 55455

Received July 24, 1995[⊗]

Abstract: Dual-level generalized transition state theory and statistical calculations based on correlated electronic structure calculations with augmented correlated basis sets are used to predict rate constants and deuterium kinetic isotope effects for the competing S_N2 and E2 reactions of ClO^- with C_2H_5Cl. The E2 reaction is favored by zero point effects despite its higher barrier. Furthermore, the entropic contribution of low-frequency transition state modes promotes the E2 reaction by about an order of magnitude at 300 K, despite nearly equal combined electronic/zero point propensities for the two reactions. The kinetic isotope effect for the E2 reaction is predicted to be 8.3 at 100 K and 3.1 at room temperature. The kinetic isotope effect of the S_N2 reaction is predicted to be surprisingly low at low temperatures (0.06 at 100 K) and 0.60 at room temperature. The activation energy for both reactions is predicted to be negative below about 900 K and positive above 1000 K. Variational effects on the location of the central dynamical bottleneck are small for both reactions.

Introduction

The factors controlling the competition between S_N2 (bimolecular nucleophilic substitution) and E2 (bimolecular elimination) reaction pathways are important for structure−activity relationships and for fundamental mechanistic physical organic chemistry. The study of gas-phase ion−molecule reactions provides a route to understanding the intrinsic factors independent of solvent effects.[1−3] The prototype case for this competition involves the attack of an alkyl halide by a nucleophilic group. For methyl halides, only the S_N2 pathway is possible. For more complicated halides, the E2 pathway is also possible and may compete with the S_N2 pathway. Experimentally it is difficult to differentiate between these two pathways since they involve not only the same reactants but also the same product ions. However, one important distinction between these two types of reactions is that the E2 reactions are believed to show high deuterium kinetic isotope effects (KIEs) at room temperature ($k_H/k_D \approx 2-6$)[1b] while the S_N2 reactions usually show slightly inverse KIEs ($k_H/k_D \approx 0.7-1.0$).[1f]

There has been little theoretical study[3] on gas-phase E2 reactions and even less study of competitive E2 and S_N2 reactions. This may be attributed to the fact that E2 reactions typically occur only in systems with quite a few atoms, making reliable *ab initio* calculations difficult or impractical. However, the study of these more complicated reactions and the causes of their rate and KIE differences at the molecular level are essential to a fundamental understanding of these important types of organic reactions.

In this article, we report structural studies of transition states and dynamical calculations of reaction rate constants and KIEs as functions of temperature for the $ClO^- + C_2H_5Cl$ reaction and its pentadeuterated analog via both the E2 and S_N2 pathways:

$$ClO^- + C_2H_5Cl \rightarrow ClOH + C_2H_4 + Cl^- \qquad (E2)$$

$$ClO^- + C_2H_5Cl \rightarrow C_2H_5OCl + Cl^- \qquad (S_N2)$$

The structural studies are based on extended-basis-set[4] electronic structure calculations including electron correlation.[5] The rate

[⊗] Abstract published in *Advance ACS Abstracts,* January 15, 1996.

(1) Recent experimental work on gas-phase S_N2 and E2 reactions: (a) DePuy, C. H.; Beedle, E. C.; Bierbaum, V. M. *J. Am. Chem. Soc.* **1982**, *104*, 6483. (b) de Koning, L. J.; Nibbering, N. M. M. *J. Am. Chem. Soc.* **1987**, *109*, 1715. (c) Lum, R. C.; Grabowski, J. J. *J. Am. Chem. Soc.* **1988**, *110*, 8568. (d) Jones, M. E.; Ellison, B. *J. Am. Chem. Soc.* **1989**, *111*, 2297. (e) DePuy, C. H.; Gronert, S.; Mullin, A.; Bierbaum, V. M. *J. Am. Chem. Soc.* **1990**, *112*, 8650. (f) Gronert, S.; Depuy, C. H.; Bierbaum, V. M. *J. Am. Chem. Soc.* **1991**, *113*, 4009. (g) Viggiano, A. A.; Morris, R. A.; Paschkewitz, J. S.; Paulson, J. F. *J. Am. Chem. Soc.* **1992**, *114*, 10477. (h) Knighton, W. B.; Bognar, J. A.; O'Connor, P. M.; Grimsrud, E. P. *J. Am. Chem. Soc.* **1993**, *115*, 12079. (i) Wladkowski, B. D.; Wilbur, J. L.; Brauman, J. I. *J. Am. Chem. Soc.* **1994**, *116*, 2471. (j) Graul, S. T.; Bowers, M. T. *J. Am. Chem. Soc.* **1994**, *116*, 3875. (k) Cyr, D. M.; Scarton, M. G.; Wiberg, K. B.; Johnson, M. A.; Nonose, S.; Hirokawa, J.; Tanaka, H.; Kondow, T.; Morris, R. A.; Viggiano, A. A. *J. Am. Chem. Soc.* **1995**, *117*, 1828.

(2) Representative recent theoretical papers on S_N2 reactions from which earlier work may be traced: (a) Zhao, X. G.; Lu, D.-h.; Liu, Y.-P.; Lynch, G. C.; Truhlar, D. G. *J. Chem. Phys.* **1992**, *97*, 6369. (b) Wang, H. B.; Zhu, L.; Hase, W. L. *J. Phys. Chem.* **1994**, *98*, 1608. (c) Wang, H. B.; Peslherbe, G. H.; Hase, W. L. *J. Am. Chem. Soc.* **1994**, *116*, 9644. (d) Boyd, R. J.; Kim, C. K.; Shi, Z.; Weinberg, N.; Wolfe, S. *J. Am. Chem. Soc.* **1993**, *115*, 10147. (e) Poirier, R. A.; Wang, W. L.; Westaway, K. C. *J. Am. Chem. Soc.* **1994**, *116*, 2526. (f) Buhl, M.; Schaefer, H. F. *J. Am. Chem. Soc.* **1993**, *115*, 9143. (g) Shaik, S.; Ioffe, A.; Reddy, A. C.; Pross, A. *J. Am. Chem. Soc.* **1994**, *116*, 262. (h) Baj, S.; Dawid, M. *Theochem* **1994**, *112*, 67. (i) Anh, N. T.; Thanh, B. T.; Thao, H. H.; Nguessan, Y. T. *New J. Chem.* **1994**, *18*, 489. (j) Glad, S. S.; Jensen, F. *J. Chem. Soc., Perkin Trans. 2* **1994**, 871. (k) Hu, W.-P.; Truhlar, D. G. *J. Am. Chem. Soc.* **1994**, *116*, 7797. (l) Deng, L. Q.; Branchadell, V.; Ziegler, T. *J. Am. Chem. Soc.* **1994**, *116*, 10645. (m) Minyaev, R. M.; Wales, D. J. *J. Phys. Chem.* **1994**, *98*, 7942. (n) Glukhovtsev, M. N.; Pross, A.; Radom, L. *J. Am. Chem. Soc.* **1995**, *117*, 2024. (o) Lucchini, V.; Modena, G.; Pasquato, L. *J. Am. Chem. Soc.* **1995**, *117*, 2297. (p) Hu, W.-P.; Truhlar, D. G. *J. Am. Chem. Soc.* **1995**, *117*, 10726.

(3) Recent theoretical study of E2 reactions: (a) Minato, T.; Yamabe, S. *J. Am. Chem. Soc.* **1985**, *107*, 4621. (b) Minato, T.; Yamabe, S. *J. Am. Chem. Soc.* **1988**, *110*, 4586. (c) Dewar, M. J.; Yuan, Y.-C. *J. Am. Chem. Soc.* **1990**, *112*, 2088. (d) Dewar, M. J.; Yuan, Y.-C. *J. Am. Chem. Soc.* **1990**, *112*, 2095. (e) Gronert, S. *J. Am. Chem. Soc.* **1991**, *113*, 6041. (f) Gronert, S. *J. Am. Chem. Soc.* **1992**, *114*, 2349. (g) Gronert, S. *J. Am. Chem. Soc.* **1993**, *115*, 652. (h) Bickelhaupt, F. M.; Baerends, E. J.; Nibbering, N. M. M.; Ziegler, T. *J. Am. Chem. Soc.* **1993**, *115*, 9160. (i) Gronert, S. *J. Org. Chem.* **1994**, *59*, 7046. (j) Glad, S. S.; Jensen, F. *J. Am. Chem. Soc.* **1994**, *116*, 9302.

(4) (a) Dunning, T. H., Jr. *J. Chem. Phys.* **1989**, *90*, 1007. (b) Woon, D. E.; Dunning, T. H., Jr. *J. Chem. Phys.*, **1993**, *98*, 1358.

0002-7863/96/1518-0860$12.00/0

constant calculations are based on the dual-level direct dynamics method[6,7] based on variational transition state theory (VTST)[8−10] and a new competitive canonical unified statistical (CCUS) model presented below (the latter being an extension of an earlier[11] unified model that did not involve competitive reactions). The KIEs and their temperature dependences are analyzed by factorization of various contributions to the CCUS rate constants.

Theory and Computational Methods

We performed extended-basis-set calculations to obtain the critical properties of the reactants, products, and transition states, in particular, their optimized geometries, Born−Oppenheimer energies, and harmonic vibrational frequencies. (The Born−Oppenheimer energy is sometimes called the classical energy; it equals the sum of the electronic energy and the nuclear repulsion.) Electron correlation effects have been included at the Møller−Plesset second-order[5] (MP2) level. The basis set used for carbon and hydrogen atoms is the correlation-consistent polarized valence double-ζ basis set (cc-pVDZ),[4a] and the basis set for oxygen and chlorine atoms is the augmented correlation-consistent polarized valence double-ζ basis set (aug-cc-pVDZ)[4] without the diffuse d functions. Thus the basis includes diffuse s and p functions on O and on both Cl atoms. The basis set size for the whole system is 115 contracted Gaussian basis functions (355 primitive Gaussian functions). In the rest of this paper we call the basis functions used for this system the ADZP basis set. These MP2/ADZP data serve as the high-level data in our dual-level dynamics calculations. The electronic structure calculations were performed using the GAUSSIAN 92[12] program on Cray X-MP-EA and Cray C90 supercomputers at the Minnesota Supercomputer Institute.

In this study only the *anti*-stereochemical mechanism of the E2 reaction is considered.

The low-level surface for the dual-level VTST calculation was obtained by neglect of diatomic differential overlap with specific reaction parameters[6,7,13] (NDDO-SRP) based on modifications of the general Austin Model 1[14] (AM1) parametrization. Interpolated corrections to the energies and vibrational frequencies of the low-level surface were calculated for reactants, products, and saddle point at the MP2/ADZP level described above. Corrections for vibrational frequencies were set to zero at the ion−dipole complexes. The correction for Born−Oppenheimer energy was also set to zero at the reactant complex and was set to the difference between the experimental energies of reaction and the NDDO-SRP value at the product complex. The dual-level dynamics VTST calculations[6,7] are designated as MP2/ADZP/// NDDO-SRP where X///Y denotes[7] single-point calculations at level X along a reaction path calculated at level Y. These dual-level dynamics calculations were performed using canonical variational theory[9,15] (CVT) with the MORATE 6.5 program[16] on the Cray C90.

The hindered-rotor approximation[17] was used for the lowest-frequency modes of the transition states for both reactions, and all other modes are treated harmonically.

A generalization of the canonical unified statistical (CUS) model[9,11] was used to calculate the final rate constants using the dual-level CVT rate constants and the ion−dipole capture rate. The CUS model is the simplest way to allow for a statistical branching probability for the reaction complex to redissociate to reactants. The generalization is called the competitive canonical unified statistical (CCUS) model, and it accounts for the two competitive ways for the ion−dipole complex of the reactants to react.

The microcanonical and canonical unified statistical methods were originally formulated for the case shown schematically in Figure 1a,[9,11b,c] and they were generalized to more complicated cases like Figure 1b in later work.[2a,p,11d] In these figures, the ordinate is the generalized transition-state-theory free energy of activation, and the abscissa is the distance along a reaction coordinate. The present situation corresponds to a case like that shown in Figure 1c, where the competitive reaction paths diverge after the initial complex. However, both reactions are sufficiently exergonic that we can neglect the product side complexes and the association bottlenecks for the reverse reactions. Thus there is negligible loss in considering the simplified case of Figure 1d for the present rate calculations. Let k_i denote the flux coefficient for a dividing surface at location i, where i = *1, C, *2A, or *2B, where the asterisk signifies a local maximum along a free energy of activation profile. In terms of these quantities the CUS rate constant k^{CUS} for case (a) is given by[9,11]

$$\frac{1}{k^{CUS}} = \frac{1}{k_{*1}} - \frac{1}{k_C} + \frac{1}{k_{*2}} \tag{1}$$

The generalization to the competitive CUS rate constant k^{CCUS} for case (d) is obtained by straightforward application of the well-known procedures for combining fluxes in parallel and series, which yields

$$\frac{1}{k_{total}^{CCUS}} = \frac{1}{k_{*1}} - \frac{1}{k_C} + \frac{1}{(k_{*2A} + k_{*2B})} \tag{2}$$

This gives the overall rate; the individual E2 and S_N2 rate constants are given by

$$k_{E2}^{CCUS} = \frac{k_{*2A}}{k_{*2A} + k_{*2B}} k_{total}^{CCUS} \tag{3}$$

and

$$k_{S_N2}^{CCUS} = \frac{k_{*2B}}{k_{*2A} + k_{*2B}} k_{total}^{CCUS} \tag{4}$$

where k_{*1} is the ion−molecule capture rate constant, k_{*2A} is the CVT rate constant for the E2 reaction, and k_{*2B} is the CVT rate constant for the S_N2 reaction. In the present case, the reactant complex is at least 5 kcal/mol lower in energy than both the reactants and the transition states so the $1/k_C$ term in eqs 1 and 2 can be neglected. All calculations are for the low-pressure limit of reaction where bimolecular collisions are not interrupted by collisions with third bodies. Note that when $k_{*2A} \ll k_{*1}$ and $k_{*2B} \ll k_{*1}$, no assumptions beyond the fundamental assumption of transition state theory are required for the above formulas to hold, but at low temperature, where $k_{*1} \ll k_{*2A}$ and $k_{*1} \ll k_{*2B}$, the treatment implicitly assumes that the system is equilibrated in the ion−dipole complex and decays to products by competitive unimolecular decay.

(5) (a) Hehre, W. J.; Radom, L.; Schleyer, P. v. R.; Pople, J. A. *Ab initio Molecular Orbital Theory*; Wiley: New York, 1986. (b) Adams, G. F.; Bent, G. D.; Bartlett, R. J.; Purvis, G. D. In *Potential Energy Surfaces and Dynamics Calculations*; Truhlar, D. G., Ed.; Plenum: New York, 1981; p 133.

(6) Hu, W.-P.; Liu, Y.-P.; Truhlar, D. G. *J. Chem. Soc., Faraday Trans.* **1994**, *90*, 1715.

(7) Corchado, J. C.; Espinosa-Garcia, Joaquin; Hu, W.-P.; Rossi, I.; Truhlar, D. G. *J. Phys. Chem.* **1995**, *99*, 687.

(8) Truhlar, D. G.; Garrett, B. C. *Acc. Chem. Res.* **1980**, *13*, 440.

(9) Truhlar, D. G.; Isaacson, A. D.; Garrett, B. C. In *Theory of Chemical Reaction dynamics*; Baer, M., Ed.; CRC Press: Boca Raton, 1985; Vol. 4, p 65.

(10) Laidler, K. J. *Chemical Kinetics*, 3rd ed.; Harper & Row: New York, 1987.

(11) (a) Hirschfelder, J. O.; Wigner, E. *J. Chem. Phys.* **1939**, *7*, 616. (b) Miller, W. H. *J. Chem. Phys.* **1976**, *65*, 2216. (c) Garrett, B. C.; Truhlar, D. G. *J. Chem.* Phys. **1982**, *76*, 1853. (d) Miller, W. H. In *Potential Energy Surfaces and Dynamics Calculations*; Truhlar, D. G., Ed.; Plenum: New York, 1981; p 265.

(12) Gaussian 92/DFT, Revision G.1: Frisch, M. J.; Trucks, G. W.; Schlegel, H. B.; Gill, P. M. W.; Johnson, B. G.; Wong, M. W.; Foresman, J. B.; Robb, M. A.; Head-Gordon, M.; Replogle, E. S.; Gomperts, R.; Andres, J. L.; Raghavachari, K.; Binkley, J. S.; Gonzalez, C.; Martin, R. L.; Fox, D. J.; Defrees, D. J.; Baker, J.; Stewart, J. J. P.; Pople, J. A., Gaussian, Inc.: Pittsburgh, PA, 1993.

(13) Gonzalez-Lafont, A.; Truong, T. N.; Truhlar, D. G. *J. Phys. Chem.* **1991**, *95*, 4618.

(14) (a) Dewar, M. J. S.; Zoebisch, E. G.; Healy, E. F.; Stewart, J. J. P. *J. Am. Chem. Soc.* **1985**, *107*, 3902. (b) Dewar, M. J. S.; Zoebisch, E. G. *J. Mol. Struct. (THEOCHEM)* **1988**, *180*, 1.

(15) (a) Garrett, B. C.; Truhlar, D. G. *J. Chem. Phys.* **1979**, *70*, 1593. (b) Garrett, B. C.; Truhlar, D. G. *J. Am. Chem. Soc.* **1979**, *101*, 4534.

(16) Hu, W.-P.; Lynch, G. C.; Liu, Y.-P.; Rossi, I.; Stewart, J. J. P.; Steckler, R.; Garrett, B. C.; Isaacson, A. D.; Lu, D.-h.; Melissas, V. S.; Truhlar, D. G. MORATE-version 6.5. *QCPE Bull.* **1995**, *15*, 26.

(17) Truhlar, D. G. *J. Comput. Chem.* **1991**, *12*, 266.

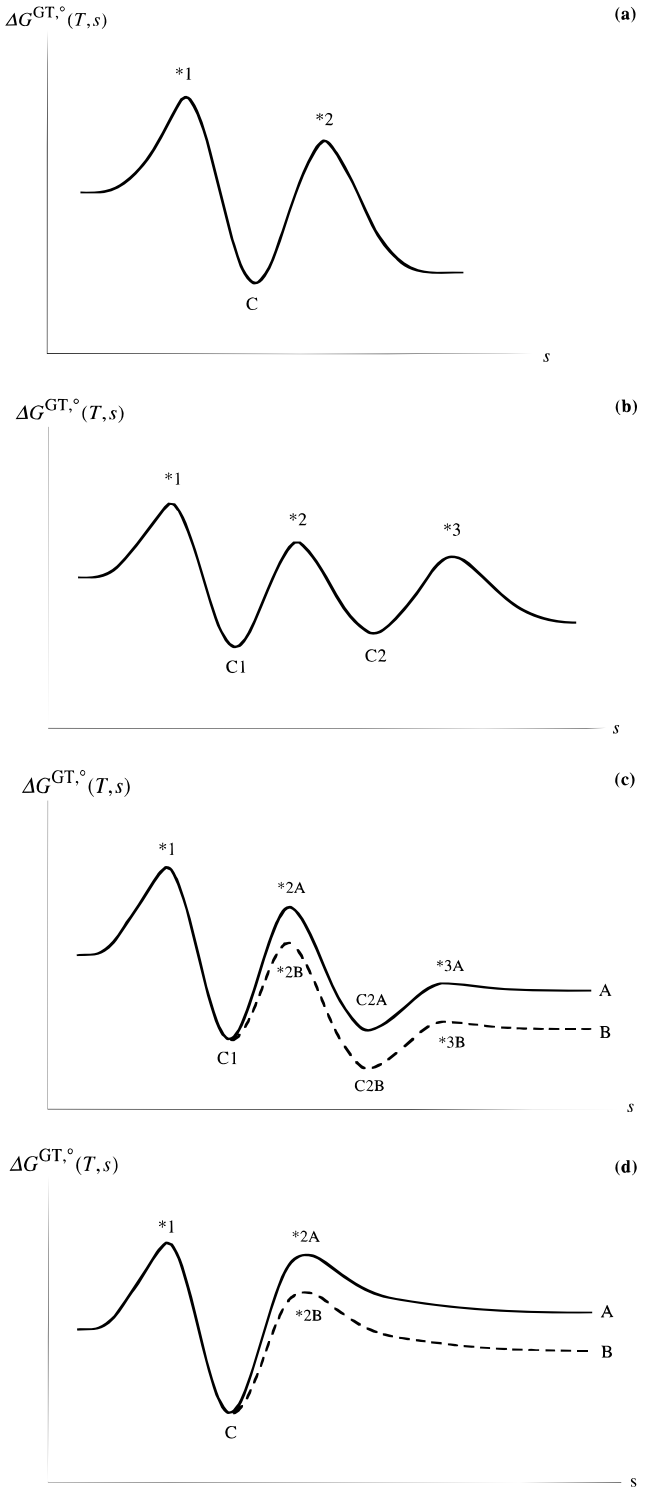

Figure 1. Schematic diagrams showing generalized transition-state (GT) standard-state (°) free energy of activation profiles vs reaction coordinates for cases discussed in the text. The dynamical bottlenecks are labeled *, the complexes are labeled C, and the products are labeled A and B.

We calculated the ion−molecule capture rates using both the Chesnavich−Su−Bowers variational transition state theory method[18] and Celli *et al.*'s method.[19] For both methods we used the experimental dipole moment[20] of 2.05 D and experimental polarizability[20] of 6.4 × 10^{-24} cm^3 for ethyl chloride. Results obtained by the two methods are compared in the Discussion section. In all CUS and CCUS calculations we used Chesnavich *et al.*'s method for the ion−molecule capture rates k_{*1}.

The kinetic isotope effect (KIE) is defined as the ratio of the rate constant of the perprotic reaction to that of the perdeuterated reaction, and it can be factored[2k,p,7,13,21] into competitive, capture, variational, translational, rotational, and vibrational contributions for either the E2 or the S_N2 reaction:

$$k_H^{CCUS}/k_D^{CCUS} = \eta_{comp}\eta_{cap}\eta_{var}\eta_{trans}\eta_{rot}^{\ddagger}\eta_{vib}^{\ddagger} \quad (5)$$

$$\eta_{comp} = \frac{k_H^{CCUS}/k_D^{CCUS}}{k_H^{CUS}/k_D^{CUS}} \quad (6)$$

$$\eta_{cap} = \frac{k_H^{CUS}/k_D^{CUS}}{k_H^{CVT}/k_D^{CVT}} \quad (7)$$

$$\eta_{var} = \frac{k_H^{CVT}/k_D^{CVT}}{k_H^{TST}/k_D^{TST}} \quad (8)$$

$$\eta_{trans} = (\mu_{rel,D}/\mu_{rel,H})^{3/2} \quad (9)$$

$$\eta_{rot}^{\ddagger} = \left[\frac{(\det \mathbf{I})_H^{\ddagger}(\det \mathbf{I})_D^{R}}{(\det \mathbf{I})_D^{\ddagger}(\det \mathbf{I})_H^{R}}\right]^{1/2} \quad (10)$$

and

$$\eta_{vib}^{\ddagger} = \frac{q_{vib,H}^{\ddagger}q_{vib,D}^{R}}{q_{vib,D}^{\ddagger}q_{vib,H}^{R}} \quad (11)$$

where μ_{rel} is the reduced mass of relative translational motion of the reactants, det **I** is the determinant of the moment of inertia tensor, a superscript R means reactant, which is ethyl chloride in eqs 10 and 11 (the det **I** of ClO^- cancels out in the KIE), a subscript H refers to the reaction with C_2H_5Cl, a subscript D refers to the reaction with C_2D_5Cl, q_{vib} is a vibrational partition function with the classical zero of energy, and ‡ denotes a quantity evaluated at the saddle point, i.e., by conventional transition state theory, which is abbreviated TST. The vibrational contribution can be further factored into contributions from low-, mid-, and high-frequency modes

$$\eta_{vib}^{\ddagger} = \eta_{low}^{\ddagger}\eta_{mid}^{\ddagger}\eta_{high}^{\ddagger} \quad (12)$$

The expressions for these contributions are similar to eq 11 but only include the frequencies in particular ranges. The KIEs and the various contributions are calculated as functions of temperature for both the E2 and S_N2 reactions, and the KIEs for the overall reaction are also calculated. In the rest of this paper when we say E2 or S_N2 reaction we usually mean the perprotic reaction unless otherwise stated.

The boundary between the high and middle frequency modes was taken as 1550 cm^{-1} for the reactions of C_2H_5Cl and 1300 cm^{-1} for the reactions of C_2D_5Cl. This places the five C−H or C−D stretches of the reactants in the high-frequency group and for the E2 reaction also retains the mode which becomes an O−H−C or O−D−C stretch at the transition state and an O−H or O−D stretch at the product in the high-frequency group. The mid-low boundary was placed at 600 cm^{-1} for C_2H_5Cl and at 515 cm^{-1} for C_2D_5Cl.

Results

The optimized geometries of reactants, products, and transition states are depicted in Figures 2−6. Partial charges on individual atoms calculated with the ChelpG[22] method using

(18) Chesnavich, W. J.; Su, T.; Bowers, M. T. *J. Chem. Phys.* **1980**, *72*, 2641.
(19) Celli, F.; Weddle, G.; Ridge, D. P. *J. Chem. Phys.* **1980**, *73*, 801.
(20) Lide, D. R., Ed. *Handbook of Chemistry and Physics*, 71st ed.; CRC Press; Boca Raton, FL, 1990.
(21) (a) Garrett, B. C.; Truhlar, D. G.; Magnuson, A. W. *J. Chem. Phys.* **1982**, *76*, 2321. (b) Tucker, S. C.; Truhlar, D. G.; Garrett, B. C.; Isaacson, A. D. *J. Chem. Phys.* **1985**, *82*, 4102. (c) Lu, D.-h.; Maurice, D.; Truhlar, D. G. *J. Am. Chem. Soc.* **1990**, *112*, 6206. (d) Zhao, X. G.; Lu, D.-h.; Liu, Y.-P.; Lynch, G. C.; Truhlar, D. G. *J. Chem. Phys.* **1992**, *97*, 6369.
(22) Breneman, C. M.; Wiberg, K. B. *J. Comput. Chem.* **1990**, *11*, 361.

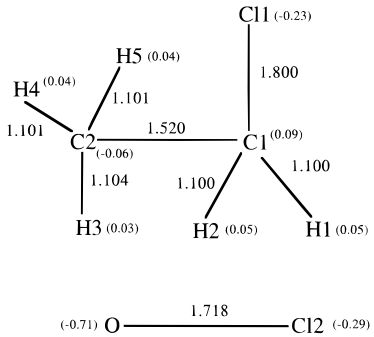

Figure 2. Geometry and partial charges (in parentheses) of the reactants. The bond lengths in the figure are in angstroms. Representative bond angles: Cl1−C1−C2 111.2°; H1−C1−H2 108.7°, C1−C2−H3 109.4°, H4−C2−H5 108.5°.

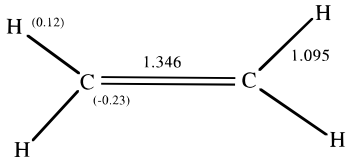

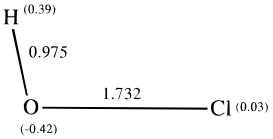

Figure 3. Geometry and partial charges (in parentheses) of the E2 products. The bond lengths in the figure are in angstroms. Representative bond angles: H−C−H 117.2°, Cl−O−H 101.3°.

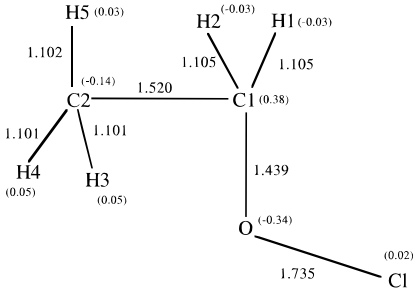

Figure 4. Geometry and partial charges (in parentheses) of the S_N2 products. The bond lengths in the figure are in angstroms. Representative bond angles: Cl−O−C1 109.9°, O−C1−C2 105.0°, C1−C2−H5 109.2°, H3−C2−H4 108.9°, H1−C1−H2 108.9°.

the MP2 density are also shown in Figures 2−6. Table 1 presents the calculated reaction energetics compared to available experimental data. The experimental Born−Oppenheimer exoergicity is obtained by

$$\Delta E = \Delta H_0^\circ - \Delta E_{ZP} \qquad (13)$$

where E_{ZP} is the zero point energy. We obtained ΔH_0° from ref 23 and ΔE_{ZP} from the MP2/ADZP calculations in the harmonic approximation. The calculated exoergicity for the E2 reaction is in good agreement (deviation of ∼1 kcal/mol) with experiment. The AM1[14] and PM3[24] values are also included in the table for comparison. A schematic energy diagram is shown in Figure 7. The new parameters of the NDDO-SRP surface are chosen by modifying the AM1 parametrization to improve the agreement of the NDDO calculations with the MP2/ADZP

(23) Chase, M. W., Jr.; Davies, C. A.; Downey, J. R., Jr.; Frurip, D. J.; McDonald, R. A.; Syverud, A. N. *J. Phys. Chem. Ref. Data* **1985**, *14*, Suppl. 1.

(24) Stewart, J. J. P. *J. Comput. Chem.* **1989**, *10*, 221.

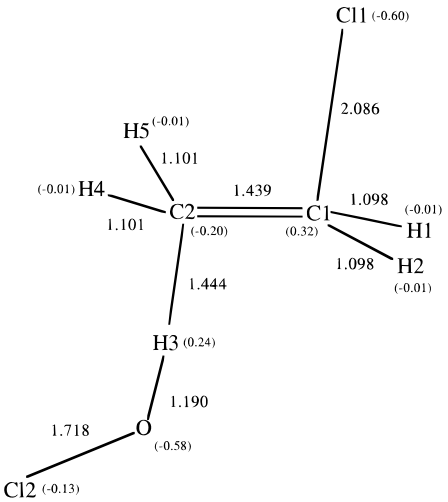

Figure 5. Geometry and partial charges (in parentheses) of the E2 transition state. The bond lengths in the figure are in Angstroms. Representative bond angles in degrees: Cl1−C1−C2 117.2, C1−C2−H3 102.1, C2−H3−O 178.8, H3−O−Cl2 106.2, H1−C1−H2 112.0, H4−C2−H5 112.1.

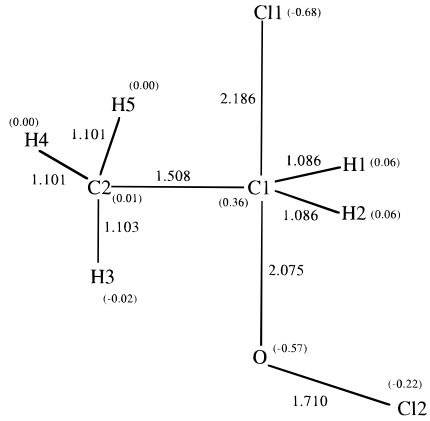

Figure 6. Geometry and partial charges (in parentheses) of the S_N2 transition state. The bond lengths in the figure are in angstroms. Representative bond angles: Cl1−C1−O 172.5°, Cl2−O−C1 110.7°, O−C1−C2 88.7°, C1−C2−H3 108.9°, Cl1−C1−C2 98.8°, H1−C1−H2 117.6°, H4−C2−H5 108.1°.

Table 1. Reaction Energetics (kcal/mol)

	E2		S_N2	
	ΔE^a	barrier height[b]	ΔE	barrier height
MP2/ADZP	−5.3	−1.3	−28.8	−4.5
AM1	−1.5	−2.6	−20.2	2.2
PM3	−13.8	−5.9	−34.0	2.1
NDDO-SRP	−4.8	−3.4	−25.5	−2.2
expt	−6.5[c]			

[a] Defined as the difference in Born−Oppenheimer energy between the products and the reactants, where a negative value means an electronically exoergic reaction. [b] Defined as the difference in Born−Oppenheimer energy between the transition state and the reactants. [c] Obtained with ΔH_0° from ref 23 and zero point energies from MP2/ADZP calculations.

results. The AM1 method was chosen as a starting point because it predicts the imaginary frequency of the transition state of the E2 reaction in much better agreement with the MP2/ADZP calculation than the PM3 method does. The parameters changed from the AM1 default values are listed in Table 2. The calculated imaginary frequencies of the transition states at different levels are summarized in Table 3. The imaginary frequencies of the S_N2 transition state from these calculations are all within 60 cm^{-1}. The calculated MP2/ADZP vibrational frequencies for stationary points are listed in Tables 4 and 5.

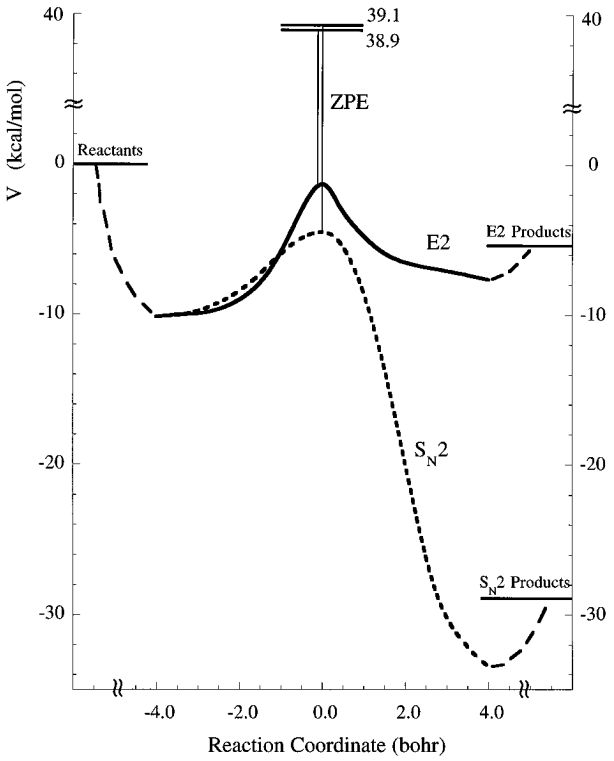

Figure 7. Reaction energetics calculated at the MP2/ADZP level. Note that reactants and products are actually at $-\infty$ and $+\infty$, respectively, so the connections between the ion−dipole complexes and these asymptotes are purely schematic, whereas the region between the complexes is taken from our dual-level calculations with the reaction coordinate scaled to a mass of 1 amu.

Table 2. AM1 Parameters (eV) Changed for the NDDO-SRP Surface

parameter	default value	new value	% changed
U_{pp}(C)	−39.6142	−39.20	1.0
U_{pp}(O)	−78.2624	−77.80	0.6

Table 3. Calculated Imaginary Frequencies (cm^{-1}) of the Transition States

	E2	S_N2
MP2/ADZP	793*i*	525*i*
AM1	856*i*	580*i*
PM3	1853*i*	526*i*
NDDO-SRP	865*i*	542*i*

The rate constants calculated by conventional transition state theory[9,10,25] (TST) at the high level and by CVT by the dual-level procedure are listed for selected temperatures in Tables 6 and 7. (Rate constants at additional temperatures are given in the supporting information.) These levels of dynamical theory depend only on the dynamical bottleneck region near the central barrier. The CUS and CCUS rate coefficients, which depend both on this region and on the association bottlenecks, are also shown in these tables along with the reaction efficiencies. The latter are defined as the ratios of the calculated CCUS rate constants to the calculated ion−dipole capture rate constants. Table 8 gives Arrhenius activation energies calculated by 2-point fits over several temperature intervals. Table 9 shows the calculated KIEs for the E2 and S_N2 reactions as functions of temperature. The calculated CCUS rate constants and KIEs as functions of temperature are also plotted in Figures 8 and 9, and the overall rates and KIEs are plotted in Figure 10. Table 10 lists the competitive, capture, and variational contributions to the KIEs, and Table 11 shows the vibrational contributions[2k,p,7,13,21] to the KIEs as functions of temperature.

The potential energy profiles of the minimum energy path

(25) (a) Johnston, H. S. *Gas-Phase Reaction Rate Theory*; Ronald Press: New York, 1966. (b) Moore, J. W.; Pearson, R. G. *Kinetics and Mechanism*, 3rd ed.; Wiley: New York, 1981.

Table 4. Calculated Harmonic Vibrational Frequencies of Reactants[a] and Products[b] (cm^{-1})

	C_2H_5Cl	C_2D_5Cl	C_2H_4	C_2D_4	C_2H_5OCl	C_2D_5OCl
ν_1	3215	2385	3311	2466	3212	2381
ν_2	3194	2372	3285	2449	3197	2369
ν_3	3190	2363	3206	2374	3141	2336
ν_4	3132	2279	3187	2301	3097	2241
ν_5	3090	2222	1688	1568	3078	2224
ν_6	1499	1207	1467	1087	1524	1237
ν_7	1492	1095	1376	1007	1500	1149
ν_8	1484	1072	1236	1000	1478	1079
ν_9	1410	1067	1066	773	1418	1072
ν_{10}	1328	1047	973	754	1384	1062
ν_{11}	1282	992	936	736	1284	1014
ν_{12}	1108	919	826	593	1184	992
ν_{13}	1089	821			1147	916
ν_{14}	1007	801			1075	908
ν_{15}	792	648			905	781
ν_{16}	709	581			833	673
ν_{17}	338	300			726	605
ν_{18}	279	279			393	362
ν_{19}					257	234
ν_{20}					249	183
ν_{21}					116	108

[a] ClO^- frequencies (cm^{-1}): 726. [b] ClOH frequencies (cm^{-1}): 726, 1226, 3774. ClOD frequencies (cm^{-1}): 722, 895, 2749.

Table 5. Calculated Harmonic Vibrational Frequencies of Transition States (cm^{-1})

	$ClO^-\cdots H_3CCH_2Cl$ (E2)	$ClO^-\cdots D_3CCD_2Cl$ (E2)	$ClO^-\cdots C_2H_5Cl$ (S_N2)	$ClO^-\cdots C_2D_5Cl$ (S_N2)
ν_1	3250	2419	3398	2541
ν_2	3200	2378	3265	2371
ν_3	3159	2303	3196	2369
ν_4	3122	2266	3183	2358
ν_5	1583	1333	3084	2216
ν_6	1515	1124	1481	1226
ν_7	1460	1079	1477	1068
ν_8	1321	1010	1462	1061
ν_9	1267	957	1384	1049
ν_{10}	1234	941	1201	968
ν_{11}	1196	910	1129	892
ν_{12}	1061	794	1098	837
ν_{13}	940	764	1042	785
ν_{14}	769	721	1016	760
ν_{15}	750	563	811	742
ν_{16}	631	546	765	586
ν_{17}	571	420	337	325
ν_{18}	464	417	319	287
ν_{19}	297	282	271	241
ν_{20}	117	115	251	241
ν_{21}	94	87	169	127
ν_{22}	60	57	86	85
ν_{23}	11	10	67	61

Table 6. Calculated Rate Constants (cm^3 $molecule^{-1}$ s^{-1}) of the E2 Reaction and the Reaction Efficiencies

T (K)	k^{TST}	k^{CVT}	k^{CUS}	k^{CCUS}	efficiency
100	1.23(−3)	8.15(−4)	3.71(−9)	3.51(−9)	0.95
150	8.19(−7)	6.34(−7)	3.11(−9)	2.93(−9)	0.94
200	2.48(−8)	2.07(−8)	2.46(−9)	2.32(−9)	0.83
250	3.39(−9)	2.95(−9)	1.37(−9)	1.32(−9)	0.52
300	9.72(−10)	8.69(−10)	6.38(−10)	6.26(−10)	0.26
400	2.38(−10)	2.18(−10)	1.98(−10)	1.97(−10)	0.09
600	8.09(−11)	7.53(−11)	7.25(−11)	7.22(−11)	0.04
1000	5.83(−11)	5.40(−11)	5.23(−11)	5.22(−11)	0.03
1500	7.46(−11)	6.84(−11)	6.56(−11)	6.53(−11)	0.04
2000	1.04(−10)	9.50(−11)	8.94(−11)	8.89(−11)	0.06

Table 7. Calculated Rate Constants (cm^3 $molecule^{-1}$ s^{-1}) of the S_N2 Reaction and the Reaction Efficiencies

T (K)	k^{TST}	k^{CVT}	k^{CUS}	k^{CCUS}	efficiency
100	4.95(−5)	4.72(−5)	3.71(−9)	2.03(−10)	0.05
150	4.02(−8)	3.85(−8)	2.89(−9)	1.78(−10)	0.06
200	1.39(−9)	1.33(−9)	9.00(−10)	1.49(−10)	0.05
250	2.09(−10)	2.01(−10)	1.86(−10)	9.00(−11)	0.04
300	6.50(−11)	6.24(−11)	6.08(−11)	4.50(−11)	0.02
400	1.78(−11)	1.71(−11)	1.70(−11)	1.54(−11)	0.01
600	6.83(−12)	6.56(−12)	6.54(−12)	6.29(−12)	0.003
1000	5.31(−12)	5.10(−12)	5.08(−12)	4.93(−12)	0.003
1500	6.93(−12)	6.66(−12)	6.63(−12)	6.36(−12)	0.004
2000	9.81(−12)	9.43(−12)	9.37(−12)	8.82(−12)	0.006

Table 8. Calculated Arrhenius Activation Energies (kcal/mol)

temp interval (K)	T_{mid}[a]	E2	S_N2	total[b]
200−250	222	−1.12	−1.00	−1.11
250−300	273	−2.22	−2.07	−2.21
300−400	343	−2.76	−2.56	−2.74
400−600	480	−2.39	−2.14	−2.37
600−800	686	−1.37	−1.11	−1.35
800−1000	889	−0.30	−0.08	−0.28
1000−1500	1200	1.33	1.52	1.35

[a] T_{mid} is the midpoint of the interval on an Arrhenius plot for the $[T_1, T_2]$ temperature interval. It is defined by $[(T_1^{-1} + T_2^{-1})/2]^{-1}$, where T_1 and T_2 are specified in the first column. [b] $k_{total} \equiv k_{E2} + k_{S_N2}$.

Table 9. KIEs Calculated by the CCUS Method

T (K)	E2	S_N2	T (K)	E2	S_N2
100	8.30	0.06	500	1.86	0.74
150	2.60	0.10	600	1.57	0.76
200	2.43	0.20	800	1.25	0.77
250	3.12	0.43	1000	1.10	0.78
300	3.10	0.60	1200	1.01	0.78
350	2.71	0.68	1500	0.94	0.79
400	2.35	0.71	2000	0.88	0.81

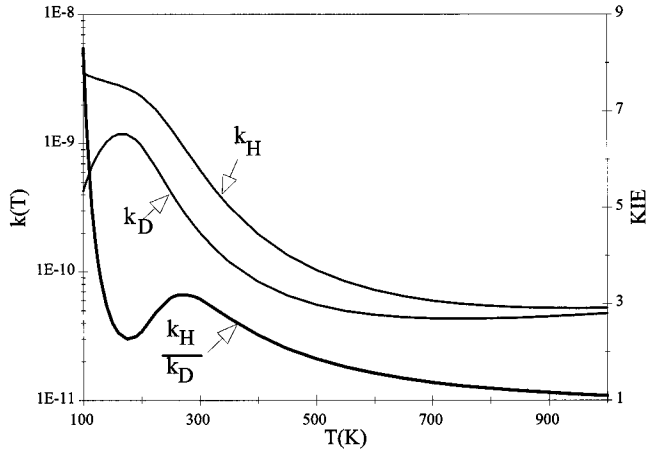

Figure 8. Calculated rate constants (in cm^3 $molecule^{-1}$ s^{-1}) and KIEs as a function of temperature for the E2 reaction.

(V_{MEP})[8,9] and the vibrationally adiabatic ground-state potential curve[9,26] (V_a^G) of the E2 and S_N2 reactions calculated with the dual-level direct dynamics method are plotted in Figures 11 and 12. The zero of energy is the same as in Figure 7.

Discussion

Ideally one would use pre-validated methods and would lead off the discussion with an estimate of the accuracy of the theoretical approaches. Unfortunately, although the reliability of *ab initio* electronic structure methods and normal mode treatments of vibrations an be gauged well from past experience

(26) Garrett, B. C.; Truhlar, D. G.; Grev, R. S.; Magnuson, A. W. *J. Phys. Chem.* **1980**, *84*, 1730, **1983**, *87*, 4554(E).

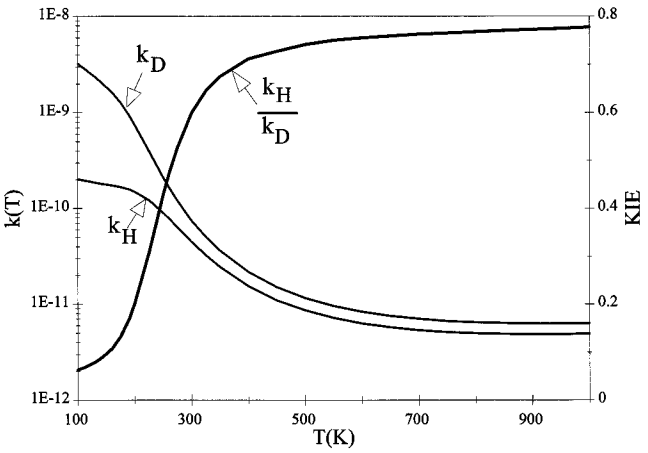

Figure 9. Calculated rate constants (in cm^3 $molecule^{-1}$ s^{-1}) and KIEs as a function of temperature for the S_N2 reaction.

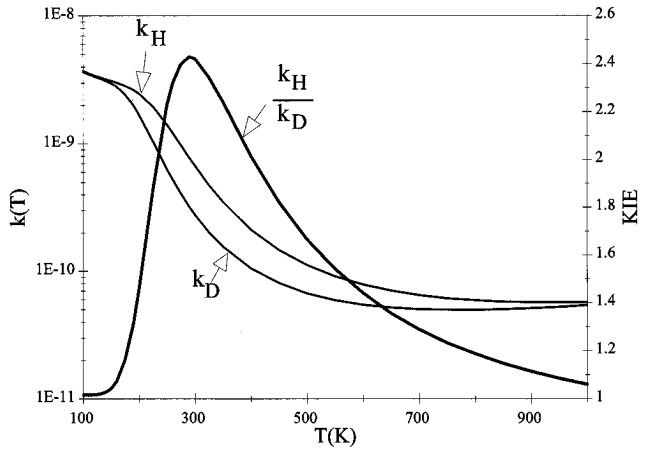

Figure 10. Calculated rate constants (in cm^3 $molecule^{-1}$ s^{-1}) and KIEs as a function of temperature for the overall reaction.

Table 10. Competitive, Capture, and Variational Contributions to the KIEs Calculated by the CCUS Method

	η_{comp}		η_{cap}		η_{var}	
T (K)	E2	S_N2	E2	S_N2	E2	S_N2
100	8.17	0.06	0.01	1.93	0.75	1.00
150	2.37	0.10	0.06	1.56	0.84	1.00
200	1.30	0.25	0.23	1.15	0.89	1.01
250	1.05	0.58	0.58	1.03	0.92	1.02
300	1.01	0.81	0.81	1.01	0.93	1.03
400	1.00	0.95	0.95	1.00	0.95	1.05
600	1.00	0.99	0.99	1.00	0.97	1.06
1000	1.00	1.00	1.00	1.00	0.97	1.08
1500	1.00	1.00	1.00	1.00	0.96	1.09
2000	1.00	1.01	1.01	1.00	0.96	1.09

for "normal" equilibrium structures, calculations on transition states have less certain validity. We believe, though, that the methods used here for structural and energetic aspects are accurate enough that the qualitative conclusions of the present paper would not change if we used even larger basis sets and more complete treatments of electron correlation. The reliability of the dynamics assumptions is even less certain. The accuracy of statistical rate theories for simple barrier reactions with a single dynamical bottleneck is well documented, but is very controversial for reactions proceeding through complexes. Statistical theories have not been applied to enough reactions with competitive reaction pathways for generalizations to be enunciated. The present predictions may even be qualitatively incorrect; that is one reason that they are interesting.

Table 11. Calculated Vibrational Contributions to the KIEs[a]

T (K)	$\eta^{\ddagger}_{vib}$	$\eta^{\ddagger}_{high}$	$\eta^{\ddagger}_{mid}$	$\eta^{\ddagger}_{low}$
		E2 Reaction		
100	68.91	67.12	4.68	0.22
150	15.17	16.52	2.79	0.32
200	6.93	8.19	2.14	0.39
250	4.25	5.38	1.82	0.44
300	3.03	4.06	1.62	0.46
400	1.95	2.85	1.40	0.49
600	1.23	1.99	1.22	0.51
1000	0.85	1.49	1.11	0.52
1500	0.73	1.31	1.07	0.52
2000	0.68	1.24	1.05	0.52
		S_N2 Reaction		
100	0.39	0.60	1.54	0.42
150	0.46	0.71	1.33	0.48
200	0.49	0.77	1.24	0.51
250	0.51	0.81	1.18	0.53
300	0.52	0.84	1.14	0.54
400	0.52	0.88	1.09	0.54
600	0.52	0.92	1.03	0.55
1000	0.52	0.96	0.99	0.55
1500	0.53	0.98	0.98	0.55
2000	0.53	0.99	0.97	0.55

[a] High-frequency modes include modes 1−5 of the transition state (Table 5) and modes 1−5 of ethyl chloride (Table 4). Low-frequency modes include modes with frequencies below 600 cm^{-1} for the C_2H_5Cl reactions and below 515 cm^{-1} for the C_2D_5Cl reactions. The rest are the middle-frequency modes.

α Effect. Although hypochlorite ion is a prototypical α nucleophile,[27] that aspect of its reactive behavior is not of concern here. We simply point out that it would be interesting to focus on the α effect in future work.

Transition State Structures. In the E2 reaction the nucleophile attacks at one of the β hydrogens of ethyl chloride. In the reaction, the C−Cl bond and one C−H bond are broken, one O−H bond is formed, and the C−C bond changes from a single bond to a double bond. From Figures 2 and 5 we see that the C−Cl and C−H bond lengths increase 0.29 and 0.34 Å, respectively, from reactant to the transition state, and the C−C bond length decreases 0.08 Å. The latter value is about half of the total decrease of 0.17 Å in passing from reactants to products. In Figure 5 we notice that the carbon (C2), hydrogen (H3), and oxygen atoms lie almost in a straight line, as found in many hydrogen transfer reactions. In particular, the C2−H3−O angle is 178.8°.

In the S_N2 reaction the nucleophile attacks at the α carbon on the opposite side of the chlorine atom. In the reaction, the C−Cl bond is broken and a C−O bond is formed. The C−Cl bond increases 0.39 Å from reactant to the transition state, and the C−O bond length decreases by 0.64 Å from the transition state to the product. In Figure 6 we see that the two carbon and the two α hydrogen (H1 and H2) atoms lie almost in a plane, and the leaving Cl (Cl1), α carbon, and oxygen atoms lie almost in a straight line. Similar transition-state geometries have been found in most previously studied S_N2 reactions.

It is also interesting to examine whether the Hammond postulate[28] holds. Applying this postulate to the present competitive E2 and S_N2 reactions would predict that the more exoergic S_N2 reaction ($\Delta E \approx -29$ kcal/mol) should have an earlier transition state than the E2 reaction ($\Delta E \approx -7$ kcal/mol). To see if this holds we examine the bond length of the C−Cl bond, which changes from 1.80 Å to ∞ in both reactions. At the saddle points this bond distance is 2.09 Å for the E2 and 2.19 Å for the S_N2 reaction. Thus the E2 saddle point is earlier, and the Hammond conjecture does *not* apply from the point of view of C−Cl bond distance. It also fails from the point of view of charge evolution at the Cl atom of ethyl chloride. In both reactions the charge at this Cl changes from −0.23 at reactants to −1.00 at products. The partial charge at this Cl is −0.60 at the E2 transition state and −0.68 at the S_N2 transition state, so again the more exoergic transition state is later. Clearly this is a very "non-Hammond" competition. Finally we consider the charge on the attacking ClO^- ion. In

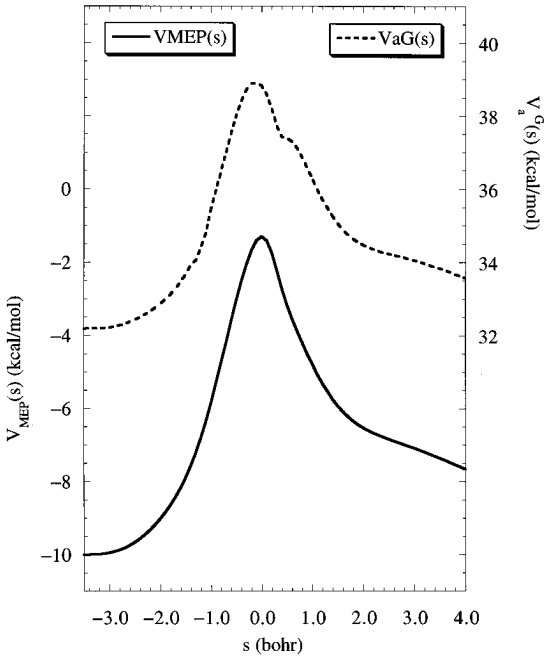

Figure 11. Calculated Born−Oppenheimer energies (V_{MEP}) and vibrationally adiabatic ground-state energies (V_a^G) along the reaction path of the E2 reaction. The reaction coordinate for Figures 11-13 was scaled to a reduced mass of 1 amu.

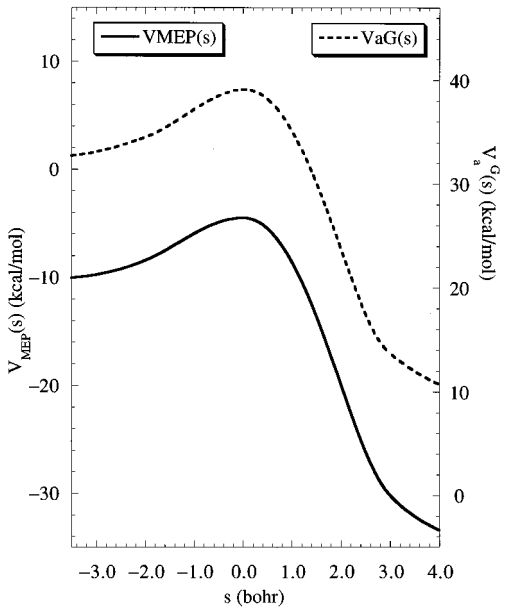

Figure 12. Calculated Born−Oppenheimer energies (V_{MEP}) and vibrationally adiabatic ground-state energies (V_a^G) along the reaction path of the S_N2 reaction.

(27) (a) Grekov, A. P.; Veselov, V. Y. *Russ. Chem. Rev.* **1978**, *47*, 631. (b) Hudson, R. F. *Chemical Reactivity and Reaction Paths*; Wiley: New York, 1974. (c) Wolfe, S.; Mitchell, D. J.; Schlegel, H. B.; Minot, C.; Eisenstein, O. *Tetrahedron Lett.* **1982**, *23*, 615. (d) DePuy, C. H.; Della, E. W.; Filley, J.; Grabowski, J. J.; Bierbaum, V. M. *J. Am. Chem. Soc.* **1983**, *105*, 2481. (e) Hudson, R. F.; Hansell, D. P.; Wolfe, S.; Mitchell, D. *J. Chem. Commun.* **1985**, 1406. (f) Fountain, K. R.; Hutchinson, L. K.; Mulhearn, D. C.; Xu, Y. B. *J. Org. Chem.* **1993**, *58*, 7883. (g) March, J. *Advanced Organic Chemistry*, 4th ed.; Wiley: New York, 1992; pp 351−352. (h) Tarkka, R. M.; Buncel, E. *J. Am. Chem. Soc.* **1995**, *117*, 1503.

(28) Hammond, G. S. *J. Am. Chem. Soc.* **1955**, *77*, 345.

the E2 reaction this changes from −1.00 at reactants to −0.39 at products, and 48% of this change is accomplished by the transition state, which is interestingly less than 50% even though the reaction is exoergic. For the S_N2 reaction the overall change in charge on ClO^- is from −1.00 to −0.32, and 31% of this change is accomplished by the transition state, so for this reaction attribute the more exoergic channel is indeed "earlier" as predicted by the Hammond postulate.

As seen in Figure 5, significant partial charges have been developed on the two carbon atoms of the E2 transition state as Cl1 and H3 leave the ethylene unit. Much of the negative charge of the reactant has been distributed over the whole transition state with the leaving chlorine atom carrying −0.60 unit of charge compared to −0.23 unit in the reactant. Significant charge transfer has to occur from the ClO^- group to C1 from the transition state to the product to change the partial charge of C1 from 0.32 to −0.23. Although part of the E2 reaction can be viewed as a proton transfer reaction, we see from Figures 2, 3, and 5 that the partial charge of H3 changes from 0.03 at the reactant to 0.24 at the transition state, and to 0.39 at the product, and thus that the hydrogen atom never carries a very high positive partial charge.

In Figure 6 we notice that only one carbon (C1) carries singificant partial charge at the S_N2 transition state. While the Cl1−C1 distance of the S_N2 transition state is 0.1 Å longer than that of the E2 transition state, the partial charge on Cl1 is 0.08 more negative. Again, some charge transfer is needed from the ClO^- group to C2 from the transition state to the product, but this charge transfer occurs to a much smaller extent than in the E2 case.

Capture Rate Constants. The capture rate constants calculated by the methods of refs 19 and 20 agreed within 5% on the average. Thus we only report the results obtained by the Chesnavich *et al.*[19] method.

Reaction Rate Constants. Since these reactions have negative barriers, an important question is whether the reaction rates are controlled by the central barrier or by the bimolecular collision rates. We notice in Tables 6 and 7 that, according to our calculation, the overall (the sum of E2 and S_N2) reaction efficiencies are high at very low temperatures, and the overall reaction rates are controlled solely by the ion−dipole capture rates at such temperatures. At approximately 300 K and higher, the central barriers begin to have significant effects on the overall reaction rates, and at high temperatures the reactions are almost totally controlled by the central barriers. The Arrhenius activation energies for the E2, S_N2, and overall reactions were computed over successive temperature intervals and are shown in Table 8. At lower temperatures, the rate constants show negative temperature dependences and thus negative activation energies because the ion−dipole collision rate decreases as the temperature increases and also because both reactions have negative barrier heights. At very high temperatures where the reactions are controlled by the central barriers the calculated rate constants show positive temperature dependences because of the vibrational partition functions and the k_BT/h term as found in previous work.[2p] Another important factor controlling the reaction rates is the competition between the E2 and S_N2 reactions, and this factor, which will be discussed later in this section, has a dramatic effect on the KIEs.

As illustrated in Figure 7, the calculated classical barrier height for the E2 reaction is 3.2 kcal/mol higher than that for the S_N2 reaction. However, the calculated vibrational zero point energy for the E2 transition state (40.1 kcal/mol) is 3.5 kcal/mol lower than that for the S_N2 reaction. As a result, these two reactions have approximately the same zero point corrected barrier heights, and they are thus expected to compete with each other. The generalized transition-state free energy of activation profile reduces at 0 K to the sum of Born−Oppenheimer energy along the reaction path and local zero point energy of the transverse modes;[15b] this sum is called the vibrationally adiabatic ground-state potential curve.[9,26] The barrier height of this curve calculated from the dual-level dynamics calculations is −4.5 kcal/mol for the E2 reaction and −4.3 kcal/mol for the S_N2 reaction. The contributions to this so-called zero point corrected barrier height (at the saddle point) are dissected in more detail in Table 12. The biggest contribution for the difference in zero point energies is mode 5 of the reactant. The zero point energy of this mode drops by 2.2 kcal/mol in proceeding from reactants to the E2 transition state because the frequency drops from 3090 to 1583 cm^{-1} where a C−H bond is attacked by ClO^-. This accounts for 63% of the difference in zero point contributions. The behavior of the frequency of this mode as a function of reaction coordinate is illustrated in Figure 13. Although the effective barrier heights for the competing reactions are very similar at 0 K, Tables 6 and 7 show that the E2 reaction rate constants are predicted to be about an order of magnitude higher than the S_N2 rate constants at higher temperature where the rates are controlled by the central barriers. This occurs mainly because the E2 transition state has lower vibrational frequencies in the transitional modes (the modes whose frequencies become zero in the reactants and products), and these frequencies correspond to larger partition functions. This is sometimes called an entropic effect. In more old-fashioned language, it corresponds to a steric factor in simple collision theory.

Adding the CCUS rates in Tables 6 and 7 yields the overall rates of reaction. Comparing to the two traditional, non-competitive methods at 300 K, conventional TST yields 1.04

Table 12. Contributions to Zero Point Corrected Barrier Height for Competitive E2 and S_N2 Reactions

energy contribution (kcal/mol)	E2	S_N2	diff
Born−Oppenheimer barrier	−1.3	−4.5	−3.2
zero point energy			
5 C−H stretches	20.5	23.1	+2.6
14 other reactant modes	19.2	19.7	+0.5
4 transitional modes	0.4	0.8	+0.4
sum	38.8	39.1	+0.3

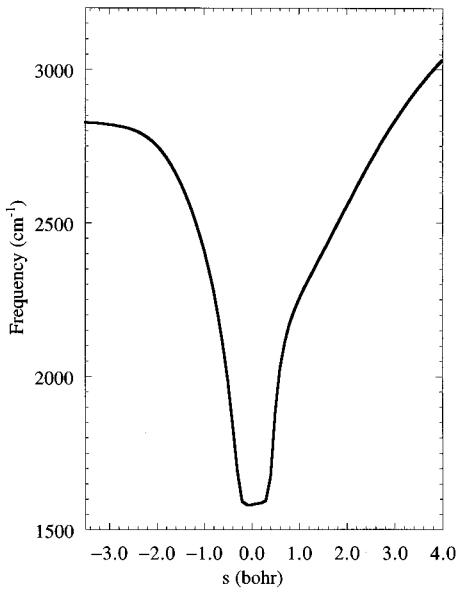

Figure 13. Calculated vibrational frequencies of ν_5 of the generalized transition state of the E2 reaction along the reaction path. This mode transforms from a C−H stretch in reactants to a ClO−H stretch in products.

$\times 10^{-9}$ cm^3 molecule^{-1} s^{-1}, CVT yields 0.93 $\times 10^{-9}$, and CCUS yields 0.67 $\times 10^{-9}$. These rate constants correspond to reaction efficiencies of 0.43, 0.39, and 0.28 respectively.

Kinetic Isotope Effects. The kinetic isotope effect for the overall reaction at 300 K decreases from 3.14 at the TST level to 2.96 at the CVT level and 2.42 at the CCUS level. The translational contributions to KIEs are independent of temperature and are 1.05 for both reactions. The rotational contributions are also independent of temperature and are 1.27 and 1.31 for the E2 and S_N2 reactions, respectively. The temperature dependences of the KIEs thus arise entirely from the competitive, capture, variational, and vibrational contributions. As shown in Tables 9 and 10, the KIEs are determined mostly by the competitive contribution at very low temperatures (see eq 6) because the CUS rate constants are almost identical to the collision rate constants (see eq 1) which are very similar for both the perprotic and perdeuterated reactions. At high temperatures, the competitive contributions are close to unity because both the CCUS and CUS rate constants converge to CVT rate constants. Also in Table 10, the capture rate contributions are very different from unity at low temperatures because of the large differences in CVT rate constants of the perprotic and perdeuterated reactions, and they are very close to unity at high temperatures because the rates are controlled by the central barriers. Table 10 also shows that most of the variational contributions are close to unity and have positive temperature dependences in most of the temperature range under study except at the highest temperatures for the E2 reaction. Tables 11 and 12 show that the vibrational contributions are normal (i.e., greater than unity) for the E2 reaction below 600 K and are inverse for the S_N2 reaction in the whole temperature range under study; this causes the differences in KIEs for the two reactions. It is noted in Table 9 that the KIEs of both reactions show strong temperature dependences at low temperatures. This is mainly because of the temperature dependences of the competitive contributions. At higher temperatures, the negative temperature dependence of the KIEs for the E2 reaction comes almost entirely from the vibrational contribution, while the S_N2 KIEs show very small temperature dependence at these temperatures because the vibrational and other contributions to the KIEs are almost constant.

Using the hindered-rotor approximation lowered the partition function of the lowest-frequency vibrational mode of the E2 transition state from 19.9 to 14.4 at 300 K and from 66.3 to 30.6 at 1000 K. This decreased the vibrational contributions, but this also increased the capture rate contributions to the KIE because the rates are smaller with the hindered rotor treatment which made the reaction more controlled by the central barrier and less controlled by the capture rate and thus made the capture rate contributions closer to unity (as shown in Tables 6, 7, and 10 that the lower the rates, the higher the capture rate contribution). The competitive contributions did not change significantly because both the perprotic and perdeuterated rate constants decreased. As a result, changing to the hindered-rotor treatment from the harmonic treatment had a relatively small effect on the KIE, and it increased the KIE by 1% at 300 K and decreased the KIE by 7% at 1000 K for the E2 reaction. The hindered-rotor treatment for the S_N2 reaction had negligible effects on both the partition functions and the KIEs.

The most important reason why the E2 reactions show large normal KIEs at room temperature is because a C−H bond is broken during the reaction, and the frequency of this C−H stretching mode decreases significantly from the reactant to the transition state, as illustrated in Figure 13. On the other hand, in the S_N2 reaction, the frequencies of the C−H stretching modes at the reacting center of the ethyl chloride increase from the reactant to the transition state, and these isotopically sensitive modes contribute inversely to the KIEs. The transitional modes also contribute strongly to the inverse KIEs. A factor analysis of the vibrational contributions to the KIEs as a function of temperature is included in Table 11.

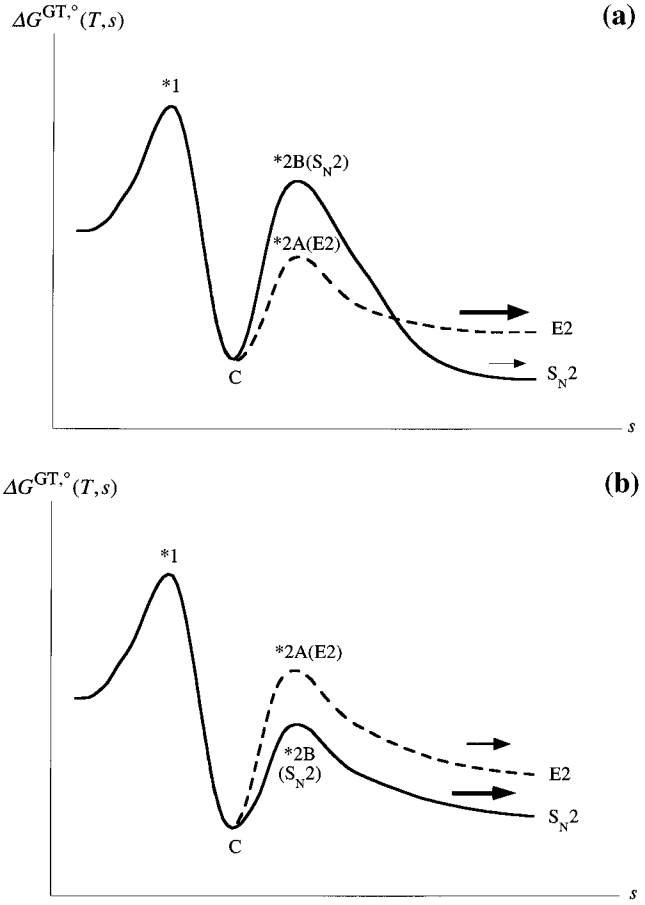

Figure 14. (a) Schematic diagram showing generalized free energy of activation profiles vs reaction coordinates for the perprotic reaction at very low temperatures. (b) Schematic diagram showing generalized free energy of activation profiles vs reaction coordinates for the perdeuterated reaction at very low temperatures.

Some very interesting phenomena are observed in Figures 8 and 9. First of all, the calculation predicts a large KIE of 8.3 for the E2 reaction and an extremely small KIE of 0.06 for the S_N2 reaction at 100 K. It is very intriguing to realize that if there were only one reaction, either E2 or S_N2, the KIE would be very close to unity at this temperature because the rate is totally controlled by the collision rate. However, since there are two channels open after the reacting system passes the (effective) collision barrier, the competitive process makes the situation more complex. Figure 14 illustrates this situation schematically. As shown in Figure 14a for the perprotic reactions, the E2 channel is much more favorable (by about a factor of 17) at this temperature so that it draws 94% of the total flux. However, in the perdeuterated reactions, as shown in Figure 14b, the S_N2 channel is more favorable (by about a factor of 8) at this temperature so that it draws 88% of the total flux. The total fluxes are about the same for both perprotic and perdeuterated reactions at this temperature. As a result the predicted temperature dependences of the KIEs are very dramatic because of the competition even though the total flux is controlled by the collision rate. For comparison, the KIEs calculated using the CVT rate constants at 100 K are 70 and 0.5 for the E2 and S_N2 reactions, respectively. At higher temperatures the reactions are controlled by the central barriers, and the KIEs are mostly determined by the calculated CVT rate constants.

It is also very interesting to note in Figure 8 that the perdeuterated E2 reaction rate constants have a positive temperature dependence below 160 K where both the collision rates and CVT rates have negative temperature dependences. This is because as the temperature goes up, the CVT rate of the perdeuterated S_N2 reaction goes down much faster than that of the perdeuterated E2 reaction does, so the perdeuterated E2 reaction gains significantly in the competition while the overall rate goes down only slightly. At higher temperatures, the temperature dependence of this rate constant also becomes negative since the overall rate goes down significantly.

It is also shown in Figure 8 that the calculated KIE of the E2 reaction decreases from 8.3 at 100 K to a minimum of 2.3 at about 175 K, it increases to a maximum of 3.2 at about 275 K, and then it decreases monotonically at higher temperatures. Figure 9 shows that the calculated KIE of the S_N2 reaction increases monotonically as the temperature goes up. As seen in Figure 10, the KIE of the overall reaction is, as expected, very close to unity at low temperatures, and it increases to a maximum of 2.4 at about 290 K and then decreases monotonically at higher temperatures.

Further Issues Relevant to Possible Future Experimental Work. It should be pointed out that the temperature (or even the existence) of the KIE maximum (or minimum) in the E2 and the overall reaction depends heavily on the absolute and relative heights of the central barriers of the E2 and S_N2 reactions. Since the barrier height is very difficult to calculate, the present estimate of the position where the maximum (or minimum) occurs may have considerable uncertainty. However, this study does demonstrate the general trends of the temperature dependences of the rate constants and the KIEs for two competitive reactions that both have negative barriers and are controlled by the collision rates at low temperatures and by the central barriers at higher temperatures. It would be very interesting to search experimentally for the non-monotonic T dependence of the rate constants and KIEs.

Bickelhaupt *et al.*[3h] studied the $F^- + CH_3CH_2F$ system using a density-functional method for electronic structure calculations and concluded that the E2 reaction should dominate in that case because of a much lower classical barrier height of −9.5 kcal/mol compared to the competing S_N2 reaction with a classical barrier height of −0.5 kcal/mol. At low temperatures the overall reaction apparently is controlled by the collision rate instead of the central barrier, and the S_N2 reaction can almost be neglected. Even though the reaction proceeds primarily via the E2 pathway, without competition from the S_N2 reaction, the overall reaction would not show significant KIEs. Glad *et al.*[3j] calculated the KIEs of the E2 reactions of ethyl chloride with 11 different nucleophiles at the MP2/6-31+G* level and with conventional transition state theory. However, many of those reactions have very low barrier heights and are totally controlled by the collision rates except at extremely high temperatures. Thus the KIEs calculated with conventional transition state theory for those reactions without considering the capture rate contribution and the competition from the S_N2 reaction do not reflect the experimentally measurable KIEs. The system in the current study was carefully chosen so that the reactions are strongly controlled by the central barriers at and above room temperature, and the two possible channels are treated competitively.

Although the $ClO^- + C_2H_5Cl$ reaction has not been studied experimentally, it has a reaction rate in the range that is accessible to experimental study with current techniques, and indeed that is the principal reason we picked it for theoretical study.

Table 13 compares some features of the $ClO^- + C_2H_5Cl$ reaction to four similar reactions that have been studied experimentally. The predicted reaction efficiency and kinetic isotope effect is not out of line with qualitative expectations for similar reactions of similar exoergicity. Experimentally, one usually can only study the sum of the E2 and S_N2 reactions (with presently available techniques). We predict that even when the S_N2 reaction is present to only the extent of 7% at 300 K, it decreases the observed KIE by 22%. Thus KIEs inferred from experiment for E2 reactions may be artifically low, and this will affect comparisons with electronic structure theory unless the S_N2 competitive path is also taken into account.

Table 13. Comparison of Theory to Experiment[a,b]

reaction	$\Delta H°$ (kcal/mol)	efficiency[c] (300 K)	k_H/k_D
E2 + S_N2			
$CF_3CH_2O^-$ + *i*-PrCl	−15	0.3	2.3
+ EtCl	−11	0.2	
$C_2F_5CH_2O^-$ + *i*-PrCl	−10	0.06	4.7
+ EtCl	−6	0.04	
ClO^- + EtCl	−8	0.28	2.4
E2 only			
ClO^- + EtCl	−8	0.26	3.1

[a] Et ≡ ethyl, *i*-PrCl ≡ isopropyl. [b] All efficiency and k_H/k_D data except those in the ClO^- + EtCl reaction are from experimental results of refs 1e and 1f. The $\Delta H°$ values are for the E2 reactions, and they are from refs 1e and 23. [c] For the perprotic reactions.

Summary

A reacting system that can go through both E2 and S_N2 channels has been studied with correlated electronic structure calculations and by the competitive canonical unified statistical model with the dual-level dynamics method. The KIEs at room temperature are "normal" for the E2 reaction and are "inverse" for the S_N2 reaction, and they are caused mainly by the C−H vibration frequency that changes along the reaction path and by the transitional modes. The calculated KIEs and their temperature dependences show very interesting behavior with very small KIE values at low temperatures for the S_N2 reaction, large KIE values at low temperatures for the E2 reaction, and a local minimum and a local maximum of the KIEs for the E2 reaction. This study also confirms the inference that the two different reaction mechanisms can be distinguished experimentally by the KIEs when the reaction is controlled by the central barrier; but when the reaction efficiency is high and the reaction is controlled by the collision rates, the overall KIEs are close to unity and they cannot be used to tell which mechanism is the dominant one. Experimental measurement of the temperature dependence of the KIEs for this system would help to assess the accuracy of the electronic structure calculations and dynamical assumptions. Experimental studies of other reactions with similar energetics would also be useful for testing the qualitative predictions about the factors controlling this kind of competition.

Acknowledgment. Helpful discussions with V. M. Bierbaum and C. H. DePuy are gratefully acknowledged. This work was supported in part by the U.S. Department of Energy, Office of Basic Energy Sciences.

Supporting Information Available: Tables of absolute energies, rate constants for C_2H_5Cl at additional temperatures, and rate constants for C_2D_5Cl (5 pages). This material is contained in many libraries on microfiche, immediately follows this article in the microfilm version of the journal, can be ordered from the ACS, and can be downloaded from the Internet; see any current masthead page for ordering information and Internet access instructions.

JA952464G